



Research Article

Effect of Vanadium on Structure and Morphology of SnO₂ Thin Films

Shawki Khalaph Muhammad¹, Ehssan Salah Hassan², Kameran Yasseen Qader³, Khalid Haneen Abass⁴, Sami Salman Chiad³, Nadir Fadhil Habubi³✉

¹Department of Physics, College of Girl Education, Kufa University, Iraq.

²Department of Physics, College of Science, Mustansiriyah University, Baghdad, Iraq.

³Department of Physics, College of Education, Mustansiriyah University, Baghdad, Iraq.

⁴Department of Physics, College of Education for Pure Sciences, University of Babylon, Iraq.

✉ Corresponding author. E-mail: nadirfadhil@uomustansiriyah.edu.iq

Received: Sep. 26, 2019; **Accepted:** Feb. 22, 2020; **Published:** Feb. 24, 2020.

Citation: Shawki Khalaph Muhammad, Ehssan Salah Hassan, Kameran Yasseen Qader, Khalid Haneen Abass, Sami Salman Chiad, and Nadir Fadhil Habubi, Effect of Vanadium on Structure and Morphology of SnO₂ Thin Films. *Nano Biomed. Eng.*, 2020, 12(1): 67-74.

DOI: 10.5101/nbe.v12i1.p67-74.

Abstract

Tin oxide was prepared by chemical methods and then doped with different weight ratios of vanadium 2wt% and 4wt%. The structural, morphological, and optical properties were studied. It was found that all the recorded films had a polycrystalline diffraction pattern and that the predominant reflection was (111) plane. The doping processes resulted in the improvement of crystalline structure and the disappearance of a number of secondary reflections and the direction of the film in a single crystalline pattern, thus reducing the values of energy gap and percentage transmittance. The morphological properties were studied by converting the three-dimensional images into graphic drawings to enable us to easily calculate surface parameters.

Keywords: Vanadium; Chemical spray; Grain bindery; Conical; Tin oxide

Introduction

The process of doping metal oxides semiconductors with the transition metals of the second group in the periodic table or their ions is considered as an important and interesting subject in many fields of applications [1], such as gas sensors [2], surface coatings, environmental and human health [3], organic pollutants and toxic water [4], photocatalysis [5], probe reaction to evaluate the catalytic activity [6], and nanocomposite or heterojunction catalysts [7]. Where a small amount of material from the transition group can have a significant and a clear effect on the properties of surface electrical conductivity [8]. Tin dioxide was doped successfully with different transition metals such as cobalt [9], nickel [10], chromium [11], iron

[12] and magnesium [13]. Where tin oxide has a wide band gap of 3.6 eV at a temperature of 300k [14], SnO₂ is a semiconductor of n type [15]. The precipitated tin oxide with vanadium was studied, which increased the sensitivity of CO gas because of the development of V⁺³, V⁺⁴, V⁺⁵ [16]. The effect of addition of vanadium to SnO₂ was also studied, and it was found that V⁺⁴ ions were the best performance of V⁺⁵ for H₂, which reduced the oxygen vacancies on the surface and reduced the degree of crystallization [17]. Vanadium was added to SnO₂ for the purpose of measuring the sensitivity of the prepared film to SO₂ sulfur dioxide at a concentration of 5 ppm. Sensitivity percentage was 70% when adding 15wt% to SnO₂ at the concentration of gas 100 ppm of SO₂. For 5 ppm of SO₂ gas, sensitivity percentage was 45% in the same doping

weight ratio [18]. The aim of this work was to prepare vanadium doped SnO_2 in order to study its structural, morphological and optical properties.

Experimental

The experimental setup was discussed elsewhere [19]. 0.1 M of $\text{SnCl}_4 \cdot 5\text{H}_2\text{O}$ was dissolved in deionized water to prepare undoped SnO_2 provided by Sigma-Aldrich – German. The doping agent was vanadium (III) chloride VCl_3 in deionized water to prepare V doped SnO_2 provided by Sigma-Aldrich – German. A few drops of HCl were added to the solution in order to get a clear solution. Substrate was glass slide. The preparation conditions: Substrate temperature was 450 °C; distance between nozzle and substrate was 29 cm; spraying period 10 s lasted by 90 s to avoid cooling; spray rate was 5 mL/min; nitrogen gas was used as a carrier gas. X-ray diffraction (XRD) (SHIMADZU XRD-6000), scanning electron microscope (SEM) (Jeol JSM 6335F), and transmission electron microscopy (TEM) (Type CM10 PW6020, Philips-Germany) were applied. Atomic force microscopy (AFM) was used to introduce surface topography using a digital tool Nanoscope III and Dimension 3100. Ultraviolet-visible spectrophotometer (UV Spectrophotometer Shimadzu Model UV-1800) was used to record the absorbance spectra in the wavelength range 200-1000 nm.

Results and Discussion

Fig. 1 represents an X-ray diffraction pattern of SnO_2 precipitated by chemical spray technique and doped with vanadium by 2 and 4wt% on the glass

substrate. It was noted from the figure that all the undoped and doped films were of a polycrystalline pattern. The dominant reflection was the (111) plane at angle $2\theta = 30.02^\circ$ that satisfied orthorhombic SnO_2 (JCPDS 29-1484) [20]. The intensity of this reflection increased with the increase of doping and decreased the full width at half maximum (FWHM) as shown in Fig. 1(a) [21] due to improvement in the crystallization. Increase in the intensity of the dominant (111) reflection was due to the fact that the ions radius of the dopant $\text{V}^{+4} = 0.58 \text{ \AA}$ occupied interstitial sites due to the small ionic radius of the dopant ion compared to the host material $\text{Sn}^{+4} = 0.71 \text{ \AA}$, and therefore moving towards superlattice, which increased the transmittance due to the increase in grain size, leading to reducing grain boundaries that acted as centers of radiation dispersion. The inset-attached shapes represented the distribution of grain size, with grain boundaries by different colors for the purpose of clarifying the increase of these grains, indicating the improvement of the crystallization with increasing the intensity of reflection and increasing the crystalline size calculated by Sherrer's formula Eq. (1) [22, 23]. Where the crystallite size increased from 19.35 to 37.78 nm when increasing the doping from 0wt% to 4wt% of vanadium, the number of secondary reflections at (020), (021), (022), (023), (041) corresponded to the angles 31.43° , 35.76° , 47.35° , 62.54° and 67.63° . All the diffraction peaks could be related to the tetragonal rutile structure of SnO_2 and no reflections from vanadium oxide phases could be noticed. It was observed that the reflection (041) was only present in the undoped SnO_2 and the reflection (022) and (023) disappeared at the 4wt% of vanadium. The reflection

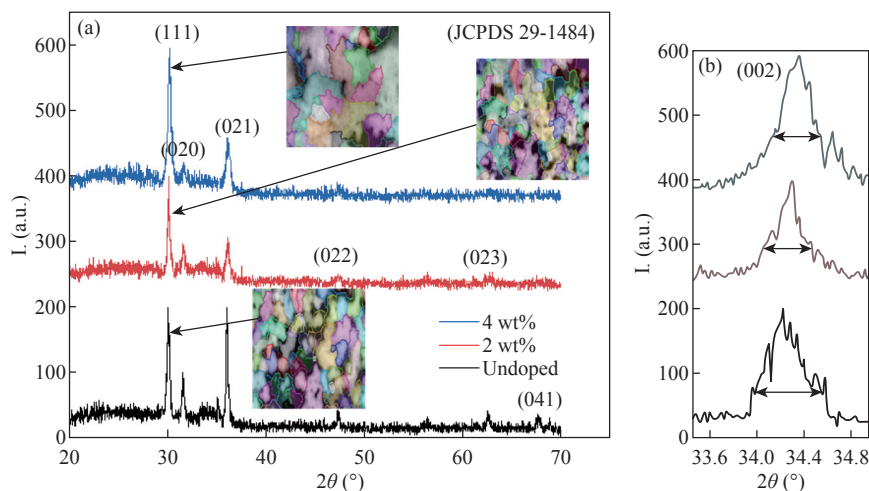


Fig. 1 (a) X-ray diffraction pattern of undoped and V doped SnO_2 ; (b) Zoom in the image of the dominant reflection.

(021) and (021) decreased their intensity with doping and the doping matter improved crystallization significantly, with the film direction to a single crystalline pattern. Fig. 2(a), (b), (c) and (d) represents the full width at half maximum, crystallite size, microstrain and the dislocation density as a function of doping weight ratios. The opposite relationship between the FWHM and crystallite size was observed from Fig. 2(a) and (b) based on the Sherrer Equation (1). Fig. 2(c) represents the microstrain that was calculated by Equation (2), which was observed to decrease with doping due to improved crystallization of the deposited film. Fig. 2 (c) represents the dislocation density that was calculated by Equation (2), which also showed the decrease in their values due to the regular arrangement of crystalline and reduced the crystalline defects in the films. The unit cell (a, b and c)

of the polycrystalline SnO₂ films with (111) orientation was calculated using Equation (4) [24] and found good agreement with those reported in JCPDS standard data as shown in Table 1.

$$D = (k\lambda)/(\beta \cos \theta) \tag{1}$$

$$\varepsilon = (\beta \cos \theta)/4 \tag{2}$$

$$\delta = 1/D^2 \tag{3}$$

$$1/d^2 = (h^2/a^2) + (k^2/b^2) + (l^2/c^2). \tag{4}$$

Fig. 3(a) represents a two-dimensional scanning electron microscope (SEM) image. Fig. 3(b) is a picture of a specific and amplified area of the film surface of Fig. 3(a) and different colors showing particle size using a professional program to calculate the surface parameters. Fig. 3(c) shows a graph of the distribution of surface heights of a specific area. All these figures described undoped thin films. It was

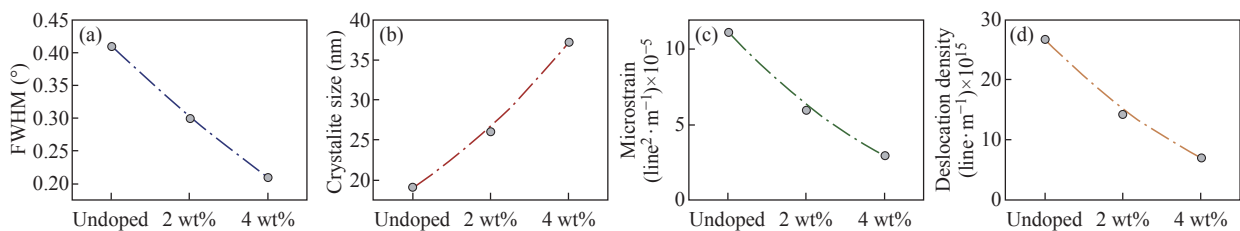


Fig. 2 (a) Full width at half maximum, (b) Crystallite size, (c) Microstrain, and (d) Dislocation density of undoped and V doped SnO₂

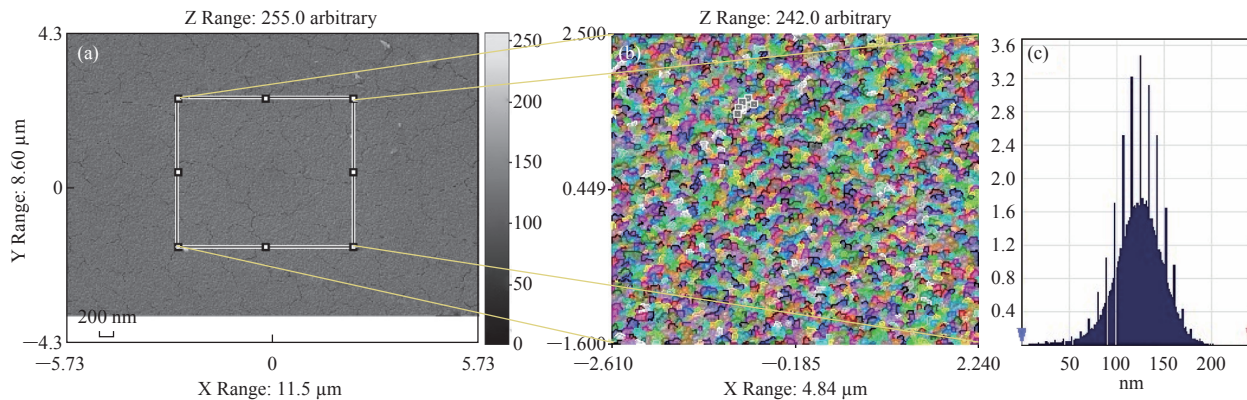


Fig. 3 Scanning electron microscope image of (a) undoped SnO₂, (b) magnified and colored image, and (c) distribution of surface heights of a specific area.

Table 1 X-ray diffraction results for undoped and V doped SnO₂ films deposited by RF magnetron sputtering at different time duration

Samples	Plane (hkl)	2θ (°)	FWHM (°)	D (nm)	a (Å)		b (Å)		c (Å)	
					Standard	Calculated	Standard	Calculated	Standard	Calculated
undoped	(111)	30.02	0.41	19.55	4.714	4.231	5.725	5.710	5.214	5.233
2 wt%	(111)	30.02	0.30	26.72	4.714	4.233	5.725	5.731	5.214	5.233
4 wt%	(111)	30.02	0.21	38.18	4.714	4.237	5.725	5.340	5.214	5.233

noticed that surface of the films was homogeneous with some cracks and that the size of particles was close to each other, as was observed from the size of the colors as about 70 nm. The height histogram indicated that the height was distributed causally at the dominant height 125 nm.

Fig. 4(a) represents a two-dimensional SEM image. Fig. 4(b) is a picture of a specific and amplified area of the film surface of Fig. 4(a) with different colors showing particle size of Fig. 4(c), a graph of the distribution of surface heights of a specific area. All these figures described 2wt% vanadium doped SnO₂ thin films. It was noticed that the surface of the films was homogeneous and the cracks became very few due to increased deflection, and that the size of the particles was close to each other. They became larger due to increased crystallization, as was observed from the size of the colors as about 80 nm. The height histogram indicated that the height was Gaussian distributed at the dominant height 140 nm.

Fig. 5(a) represents a two-dimensional SEM image.

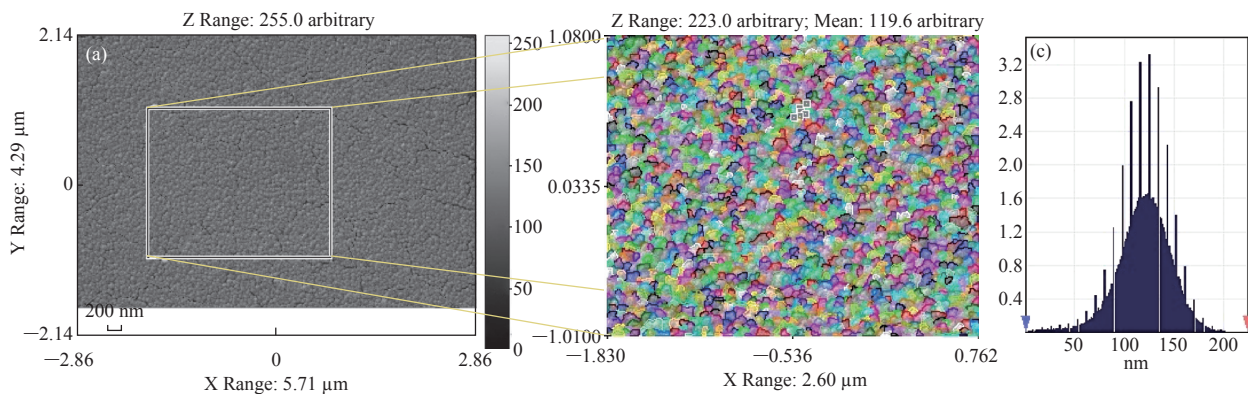


Fig. 4 Scanning electron microscope image of (a) 2wt% doped SnO₂, (b) magnified and colored image, and (c) distribution of surface heights of a specific area.

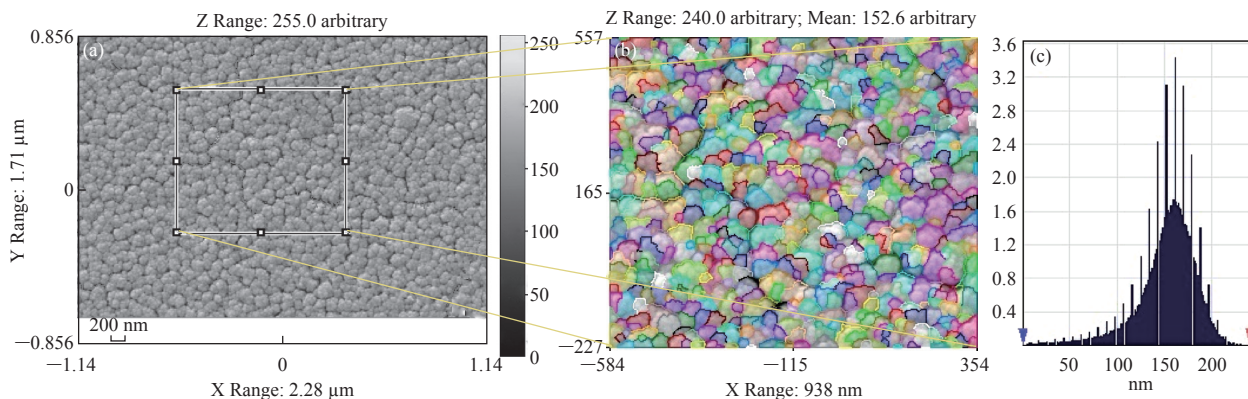


Fig. 5 Scanning electron microscope image of (a) 4wt% doped SnO₂, (b) magnified and colored image to determine particle sizes, and (c) distribution of surface heights of a specific area.

Fig. 5(b) is a picture of a specific and amplified area of the film surface of Fig. 5(a) and different colors showing particle size of Fig. 5(c), a graph of distribution of surface heights of a specific area. All these figures were for 4wt% vanadium doped SnO₂. It was noticed that the surface of films was homogeneous, free of cracks and that the size of particles was close to each other. They became larger due to increased crystallization, as was observed from the size of the colors as about 100 nm. The height histogram indicated that the height was Gaussian distributed at the dominant height 160 nm. Fig. 6 represents images of transmission electron microscopy (TEM). Fig. 6(a) represents undoped samples. It was noted that the shape was spherical with the particle size of 20 - 30 nm. It was noted that the particle size changed to 30 - 40 nm because of the change in the percentage of V doped SnO₂, as shown in Fig. 6(b) and (c).

Fig. 7(a) represents three-dimensional images of the undoped tin oxide. Fig. 7(b) is a cross-section of the x-axis in Fig. 7(a). From the undoped model in Fig.

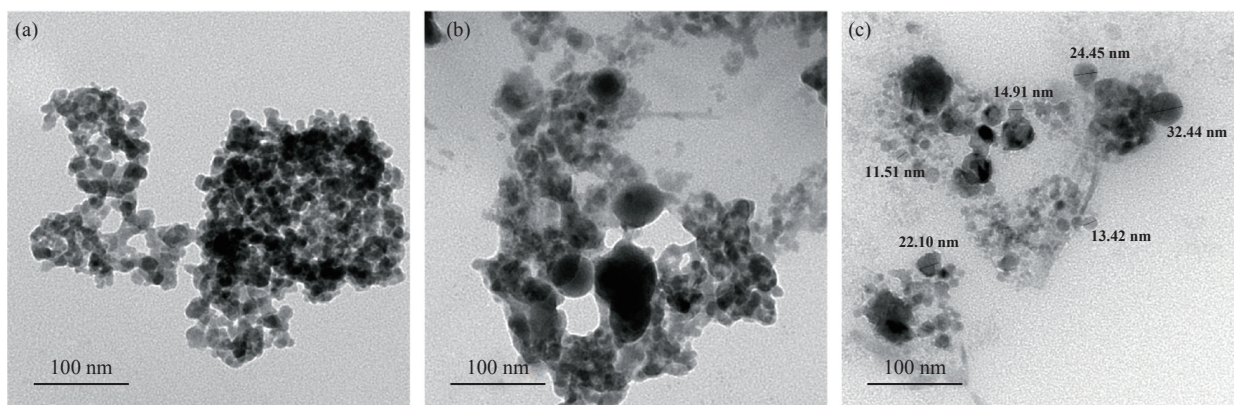


Fig. 6 Transmission electron microscopy image of (a) undoped SnO₂, (b) 2% V doped SnO₂, and (c) 4% V doped SnO₂.

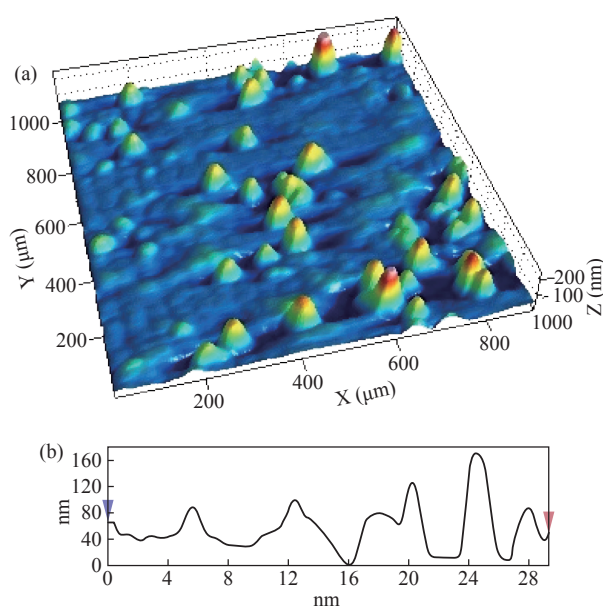


Fig. 7 Atomic force microscopy (AFM) image of undoped SnO₂: (a) 3D image 2 × 2 μm, and (b) X-Y scaling for inspection area.

7(a), we observed a number of conical nanostructures on the base, and the number of these structures was small in the measured area (1000 × 1000 μm). The topography of the X-axis in Fig. 7(b) and of its specific length was observed; the high conical shapes were between 80 - 160 nm, and the diameter of the base was 2 - 4 nm. This method is very accurate in converting three-dimensional shapes into diagrams,

Fig. 8(a) represents a three-dimensional image of the model with 2wt% vanadium, increasing the height of the conical nanostructure as well as increasing their number. The conical shape that was prevalent in the undoped SnO₂ disappeared to be replaced by structures in the form of mountain chains. In Fig. 8(b), the X-axis and a certain distance of 20 nm indicated that the

diameter of these shapes became smaller at its base as of 2 nm, and its height was greater than 200 nm due to the improved crystallization and the increased reflection intensity of XRD pattern.

Fig. 9(a) represents a three-dimensional image of the model doped with 4wt% vanadium; notes of the nanostructure increased with the height, increased the length of mountain chains, and filled the surface of the film with these structures. X-axis in Fig. 9(b) depicts the specific length of the model. It was noticed that the height of these shapes was still 200 nm, but it was becoming more like a vertical rod from the base of the substrate with a diameter of 5 - 10 nm.

Fig. 10 represents the transmittance percentage values of the undoped films, and doped films deposited by chemical spray method, and the transmittance

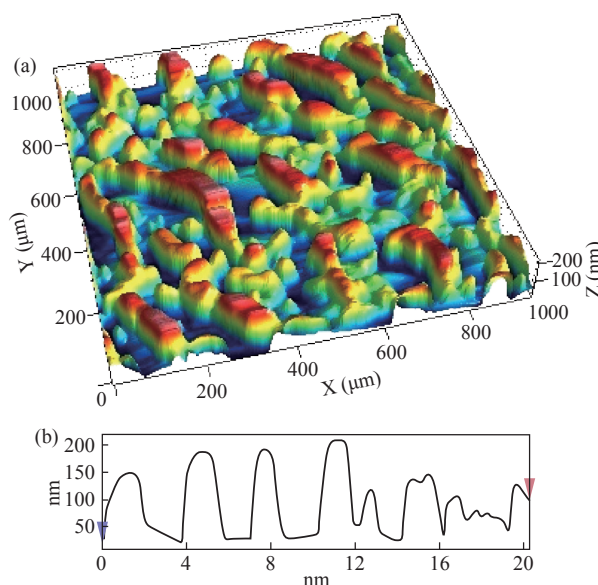


Fig. 8 Atomic force microscopy image of the 2wt% SnO₂: (a) 3D image (2×2) μm; (b) XY scaling for inspection area.

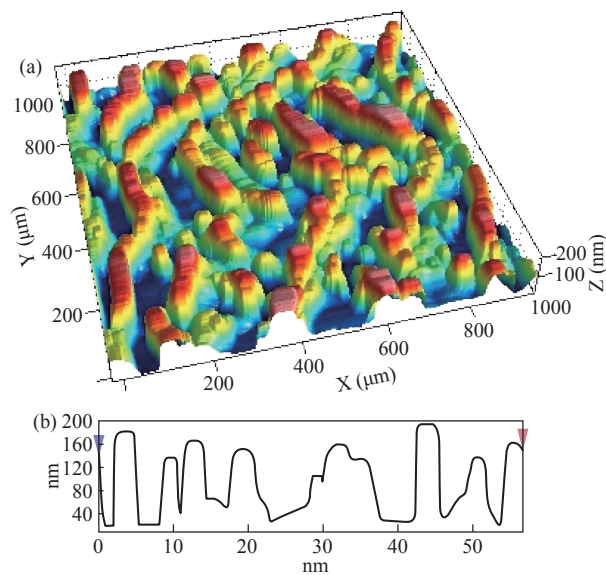


Fig. 9 Atomic force microscopy image of the 4wt% SnO₂: (a) 3D image 2 × 2 μm; (b) X-Y scaling for inspection area.

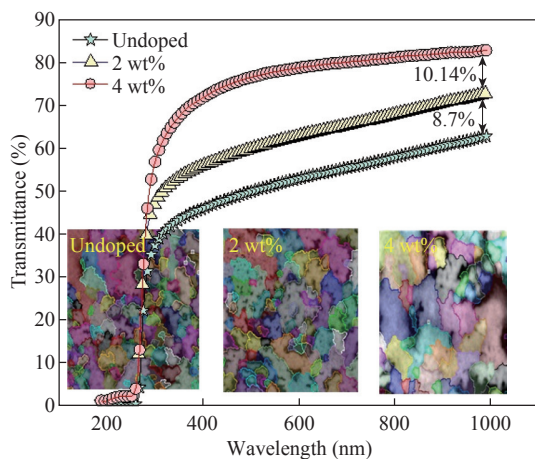


Fig. 10 Transmittance spectrum of the undoped and V doped SnO₂ films deposited by spray pyrolysis technique (SPT).

increase from 63.10% to 83.14% was observed when increasing the doping weight ratio from 0.4wt% to 4wt%. The difference in the transmittance percentage between the two successive models was about 8% - 10%. This transmittance was in the infrared, visible and ultraviolet regions. The absorption edge values for all the models were at 275 nm. The shapes attached in Fig. 11 are for surface layer, and the record shows increasing grain size with increased doping weight ratio and thus reduction of grain boundaries that acted as scattering centers of dispersion of incident radiation. Fig. 11 represents the values of the direct energy gap, which was calculated from Equation 5 [25], by plotting the values of $(\alpha h\nu)^2$ as a function of the fallen photon energy. The linear relationship between $(\alpha h\nu)^2$ and $h\nu$ could be observed in high

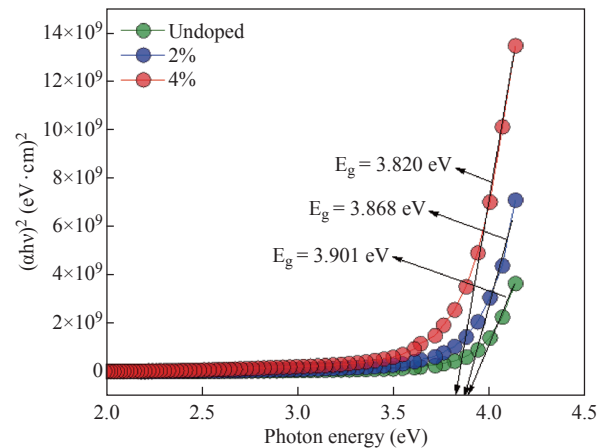


Fig. 11 Optical energy gap of the undoped and V doped SnO₂ films deposited by spray pyrolysis technique.

energy area of 8 - 10 (eV/cm)². By extrapolating the linear behavior of the curve, which represented the energy needed for the electron to move from valence band (VB) to conduction band (CB) [26]. Its value was 3.82 eV for the undoped model and decreased to 3.54 eV for the film of 2wt% and then 3.48 eV for the 4wt% film. The decreases in the energy gap values were due to secondary energy levels as vanadium reduction as well as small crystalline defects of the prepared films.

$$(\alpha h\nu) = b (h\nu - E_g)^n, \quad (5)$$

where $h\nu$ is the photon energy, n is an index related to the density of state ($n = 1/2$ for direct transition and $n = 2$ for indirect transition [27]), and E_g is the optical band gap of the semiconductor.

Fig. 12 represents the mathematical model of the experimental transmittance values of the undoped SnO₂ and vanadium doped model. It is noted from the figure that the high congruence existed between

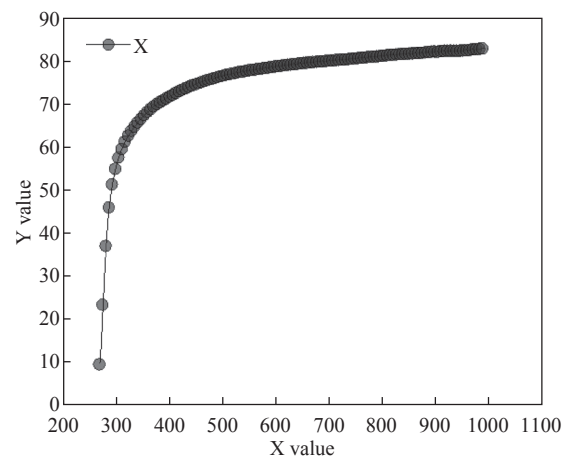


Fig. 12 The mathematical model of the experimental transmittance.

Table 2 a, b, c, d and e values for mathematical models of the transmittance

Exponential (a, b, c, d and e) $y = a + b/x + c/x^2 + d/x^3 + e/x^4$						
Coefficient of determination (r^2) 0.9826434567						
a	37.58556758	3.514706514	10.69379973	30.68528602	44.48584914	0.00000
b	84195.32845	7247.701779	11.61683124	69966.20783	98424.44907	0.00000
c	-8.9654e+07	5.29754e+06	-16.9237190	-1.0005e+08	-7.9254e+07	0.00000
d	3.41614e+10	1.63239e+09	20.92721012	3.09566e+10	3.73662e+10	0.00000
e	-4.4786e+12	1.79858e+11	-24.9009809	-4.8317e+12	-4.1255e+12	0.00000

Table 3 a, b and c value for mathematical models of the energy gap

Exponential (a, b and c) $y = a + b \times \text{Exp}(-x/c)$						
Coefficient of determination (r^2) 0.9954478797						
a	2.6258e+07	2.71663e+06	9.665647820	2.08783e+07	3.16377e+07	0.00000
b	0.002248271	0.000778029	2.889702825	0.000707563	0.003788979	0.00459
c	-0.14707494	0.001830076	-80.3654678	-0.15069898	-0.14345089	0.00000

mathematical model and experimental values where the mathematical model was set as in Equation (6). Table 2 represents the values of the variables a, b, c, d and e in the mathematical equation.

$$Y = (a+b)/x + c/x^2 + d/x^3 + e/x^4 \tag{6}$$

Fig. 13 represents the mathematical model of the experimental energy gap values and of the non-doped and vanadium doped model. It is noted from the figure that a high congruence existed between the mathematical model and experimental values where the mathematical model was set as in Equation (7).

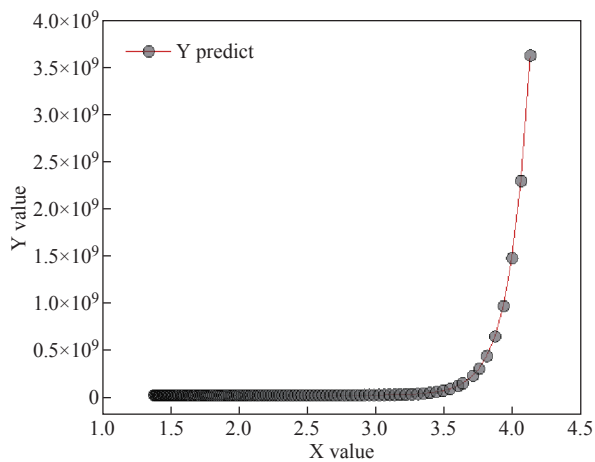


Fig. 13 The mathematical model of the experimental energy gap value.

Table 3 represents the values of the variables a, b and c in the mathematical equation.

$$Y = a + b \text{Exp}(-x/c) \tag{7}$$

Conclusions

The process of doping tin oxide with vanadium led to improving crystal structure to a degree that all numbers of secondary reflections disappeared and the intensity of the dominant reflection increased with a decrease in the transmittance percentage and the energy gap. The energy gap decreased from 3.82 eV for pure SnO₂ thin film to 3.48 eV for 4wt.% vanadium doped SnO₂ film.

Acknowledgments

Authors would like to extend their thanks and gratitude to the Department of Physics at the College of Science of the Mustansiriyah University and the Department of Physics at the College of Education of the Mustansiriyah University.

References

[1] S. Lany, Semiconducting transition metal oxides. *J. Phys.: Condens.*, 2015, 27: 283203.

- [2] C.T. Wang, M.T. Chen, and D.L. Lai, Vanadium tin oxide nanoparticles with gas sensing and catalytic activity. *Journal of the American Ceramic Society*, 2011, 94(12): 4471- 4477.
- [3] T.C. Chang, X. Cao, S.H. Bao, et al., Review on the thermochromic vanadium dioxide based smart coatings: From lab to commercial application. *Adv. Manuf.*, 2018, 6(1): 1-19.
- [4] M. Wei, X.L. Peng, Q.S. Liu, et al., Nanocrystalline TiO₂ composite films for the photodegradation of formaldehyde and oxytetracycline under visible light irradiation. *Molecules*, 2017, 22(6): 950.
- [5] C.V. Reddy, B. Babu, S.V.P. Vattikuti, et al., Structure and optical properties of vanadium doped SnO₂ nanoparticles with high photocatalytic activities. *Journal of Luminescence*, 2016, 179: 26-34.
- [6] C.T. Wang, M.T. Chen, and D.L. Lai, Surface characterization and reactivity of vanadium tin oxide nanoparticles. *Applied Surface Science*, 2011, 257: 5109-5114.
- [7] K.H. Abass, M.K. Mohammed, Abrication of ZnO:Al/Si solar cell and enhancement its efficiency via Al-doping. *Nano Biomed. Eng.*, 2019, 11(2): 170-177.
- [8] D. Todoran, R. Todoran, Z. Szakács, et al., Electrical conductivity and optical properties of pulsed laser deposited LaNi₃ nanoscale films. *Materials*, 2018, 11(8): 1475.
- [9] A. Bouaine, N. Brihi, G. Schmerber, et al., Structural, optical, and magnetic properties of Co-doped SnO₂ powders synthesized by the coprecipitation technique. *J. Phys. Chem.*, 2007, 11(17): 2924-2928.
- [10] M. Kuppam, S. Kaleemulla, N.M. Rao, et al., Structural and magnetic properties of Ni doped SnO₂. *Advances in Condensed Matter Physics*, 2013, 2014: 5.
- [11] R.R. Kasar, S.R. Gosavi, A. Ghosh, et al., Influence of Cr doping on structural, morphological and optical properties of SnO₂ thin film prepared by spray pyrolysis technique. *IOSR Journal of Applied Physics*, 2015, 7(1): 21-26.
- [12] K.A.Navneet, G.P. Singh, V. Singh, et al., Optical and structural properties of Fe-doped SnO₂ nanoparticles prepared by Co-precipitation method. *AIP Conference Proceedings*, 2016, 1728: 020055.
- [13] R.P. Harshad, Z.V.P. Murthy, Vanadium-doped magnesium oxide nanoparticles formation in presence of ionic liquids and their use in photocatalytic degradation of methylene blue. *Acta Metallurgica Sinica (English Letters)*, 2016, 29: 253-264.
- [14] R.C. Abruzzia, M.J.R. Piresa, B.A. Dedavida, et al., Application of SnO₂ nanoparticles and zeolites in coal mine methane sensors. *Mat. Res.*, 2019, 22(1): 1.
- [15] G.F. Fine, L.M. Cavanagh, A. Afonja, et al., Metal oxide semi-conductor gas sensors in environmental monitoring. *Sensors*, 2010, 10(6): 5469-5502.
- [16] T.V.K. Karthik, M.I.L. Olvera, A. Maldonado, et al., Gas sensing properties of pure and Cu-incorporated SnO₂ nanoparticles a study of Cu-induced modifications. *Sensors*, 2016, 16: 1283.
- [17] S.F. Olive-Méndez, C.R. Santillán-Rodríguez, R.A. González-Valenzuela, et al., Role of vanadium ions, oxygen vacancies, and interstitial zinc in room temperature ferromagnetism on ZnO-V₂O₅ nanoparticles. *Nanoscale Research Letters*, 2014, 9(1): 169.
- [18] Y. Wu, H. Zhang, Y. Liu, et al., Synthesis and gas sensing properties of single La-doped SnO₂ nanobelts, sensors. *Sensors (Basel)*, 2015, 5(6): 14230-14240.
- [19] R.H. Bari, S.B. Patil, and A.R. Bari, Spray pyrolysed prepared CuO-ZnO nanocomposites thin films for ethanol sensor. *Materials Focus*, 2014, 3: 119-124.
- [20] C.D. Gu, H. Zheng, X.L. Wangab, et al., Superior ethanol-sensing behavior based on SnO₂ mesocrystals incorporating orthorhombic and tetragonal phases. *RSC Adv*, 2015, 5: 9143.
- [21] S. Pati, P. Banerji, and S.B. Majumder, Properties of indium doped nanocrystalline ZnO thin films and their enhanced gas sensing performance. *RSC Adv*, 2015, 5: 61230.
- [22] C.A. Santos, L.I. Zawislak, E.J. Kinast, et al., Crystal chemistry and structure of the orthorhombic (Fe,Mn)(Ta,Nb)₂O₆ family of compounds. *Braz. J. Phys*, 2001, 31: 4.
- [23] E.S. Hassan, T.H. Mubarak, K.H. Abass et al., Structural, morphological and optical characterization of Tin doped zinc oxide thin film by SPT. *Journal of Physics: Conference Series*, 2019, 1234: 012013.
- [24] H. Morkoç, Ü. Özgür, *Zinc oxide: Fundamentals, materials and device technology*. Wiley, 2009.
- [25] S.S. Chiad, K.H. Abass, T.H. Mubarak, et al., Fabrication and study the structure, optical and dispersion parameters of PMMA with InCl₃ additive. *Journal of Global Pharma Technology*, 2019, 11(4): 369-374.
- [26] A.A. Khadayeir, E.S. Hassan, S.S. Chiad, et al., Structural and optical properties of Boron doped cadmium oxide. *Journal of Physics: Conference Series*, 2019, 1234: 012014.
- [27] D.M.A. Latif, S.S. Chiad, M.S. Erhayief, et al., Effects of FeCl₃ additives on optical parameters of PVA. *Journal of Physics: Conf. Series*, 2018, 1003: 012108.

Copyright© Shawki Khalaph Muhammad, Ehssan Salah Hassan, Kameran Yasseen Qader, Khalid Haneen Abass, Sami Salman Chiad, and Nadir Fadhil Habubi. This is an open-access article distributed under the terms of the Creative Commons Attribution License, which permits unrestricted use, distribution, and reproduction in any medium, provided the original author and source are credited.